Structure and mechanism of ergothionase from *Treponema denticola*

Alice Maurer,[a,b] Florian Leisinger,[a,b] David Lim [a] and Florian P. Seebeck[a]*

Abstract: Ergothioneine is a sulfur-containing histidine derivative that emerges from microbial biosynthesis and enters the human body via intestinal uptake and regulated distribution into specific tissues. While the proteins involved in biosynthesis and uptake are well characterized, less is known about the degradative pathways of ergothioneine. In this report we describe the crystal structure of the active form of ergothionase from the oral pathogen *Treponema denticola* in complex with the substrate analog desmethyl-ergothioneine sulfonic acid. This enzyme catalyzes 1,2-elimination of trimethylamine from ergothioneine and its oxidation product ergothioneine sulfonic acid using a unique mode of substrate activation combined with acid/base catalysis. This structural and mechanistic investigation revealed four essential catalytic residues that are strictly conserved in homologous proteins from common gastrointestinal bacteria and numerous pathogenic bacteria, suggesting that bacterial activity may play an important role in determining the availability of ergothioneine in healthy and diseased human tissue.

Ergothioneine (**1**, Figure 1) is a ubiquitous natural product that is increasingly recognized as an important micronutrient for humans. A growing body of research implicates **1** as a protectant against ailments such as inflammatory, cardiovascular or infectious diseases, cancer and neurodegeneration. [1] In spite of these intriguing leads, the molecular mechanisms by which **1** unfolds its protective activities are unknown. Because animals do not produce **1** themselves, the tissue concentration of this compound critically depends on the dietary supply, the absorption in the intestine, systemic distribution and the rates at which this micronutrient is lost by secretion or by degradation. Intestinal absorption occurs via the highly selective ergothioneine transporter ETT.[2] Distribution of **1** into specific cell-types or tissues such as red blood cells, bone marrow, liver, or kidney is governed by transcriptional regulation of the ETT-coding gene SLC22A4.[3] Up-regulation of this gene was also observed as a response to tissue damage,[1c, 4] suggesting that the active control of ergothioneine levels may be part of an adaptive cytoprotective system.[1b] This specific and possibly dynamic system for uptake and distribution provides strong evidence that **1** plays an integral and dose-dependent role in the human body, and might be considered as a vitamin.[5]

[a] A. Maurer, F. Leisinger, Dr. D. Lim and Prof. Dr. F.P. Seebeck*
Department for Chemistry
University of Basel
Mattenstrasse 24a, 4002, Basel, Switzerland
E-mail: florian.seebeck@unibas.ch
[b] equal contribution

Supporting information for this article is given via a link at the end of the document.

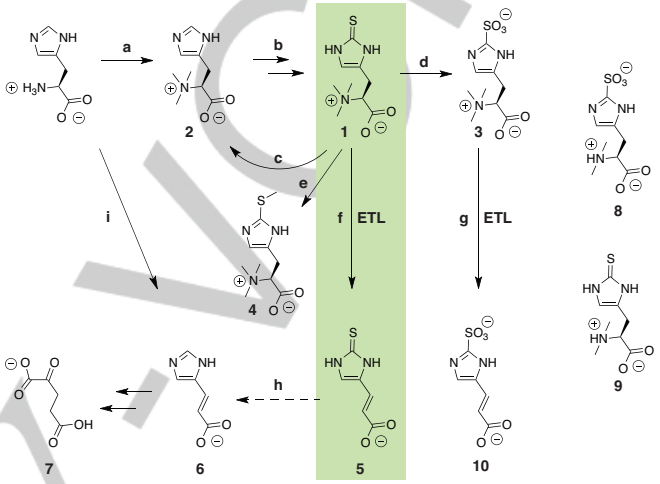

Figure 1. Ergothioneine metabolism: a, b) Biosynthesis of ergothioneine (**1**); c, d) Oxidative degradation of **1**; e) Methylation of **1** by an unknown methyl donor; f, g: ETL-catalyzed elimination of trimethylamine from **1** and **3**; h) Desulfurization of **5** and **10** by unknown enzymes could form urocanate (**6**), which is degraded to the citric acid cycle component α-ketoglutarate (**7**). i) Histidine ammonia lyase (HAL)-catalyzed degradation of histidine.

Ergothioneine enters the food chain by fungal and bacterial biosynthesis, followed by absorption or ingestion by plants and animals.[1a] Identification of ergothioneine biosynthetic enzymes revealed that most fungi and many bacteria, including most actinobacteria and cyanobacteria produce **1** from histidine, via trimethylation of the α-amino group to form N-α-trimethyl histidine (**2**), followed by attachment of a sulfur atom to the imidazole side chain (Figure 1).[6] Mechanistic and structural characterization of the key enzymes along these pathways made it possible to identify ergothioneine biosynthetic genes from genomic data with considerable certainty.[7]

The degradative pathways of **1** are more complex and less well understood. Reactive oxygen species can oxidize **1** to the corresponding sulfonic acid (**3**), or cause oxidative desulfurization (Figure 1).[8] Another pathway is methylation by an unknown methyl donor to form S-methyl ergothioneine (**4**). So far, there is no evidence that these reactions are catalyzed by specific enzymes and hence these pathways have no direct genetic footprint. On the other hand, the discovery of ergothioneine degrading activity in Enterobacteria,[9] and the identification of a specific enzyme from *Burkholderia sp.* that cleaves **1** into trimethylamine and thiourocanic acid (**5**) (Ergothioneine Trimethylammonia Lyase, *Bu*ETL) provided early evidence that degradation of **1** is also a genetically traceable process.[10]

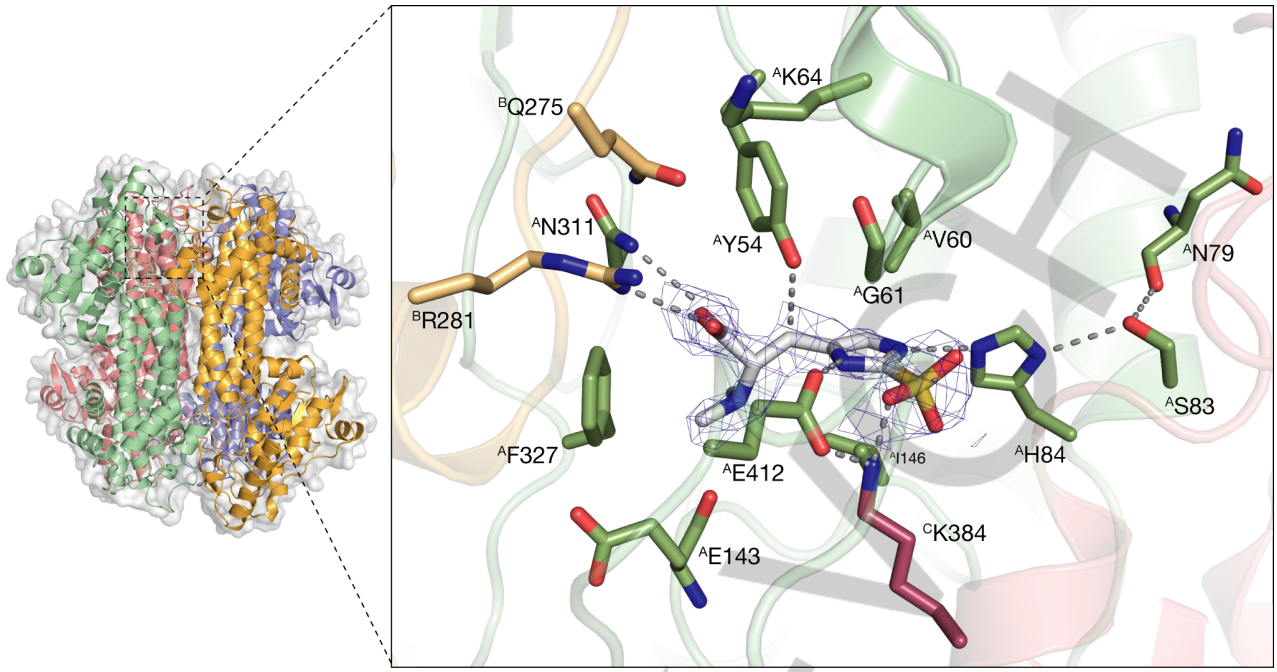

Figure 2. *Td*ETL homotetramer (left) with a close-up view into active site A in complex with *des*methyl-ergothioneine sulfonic acid (**8**, right). Active site residues and **8** are shown in stick representation and color coded according to monomer (A: green, B: orange, C: red). The 2m|F_0| - D|F_c| omit map for **8** is contured at σ-level = 1.0.

This realization raised the intriguing possibility that the concentration of **1** in food products, in the gastrointestinal tract and in specific tissues may also depend on bacterial activity. To enable identification of ETL-coding genes in bacteria we examined the crystal structure and catalytic mechanism of ETL from the pathogenic oral spirochete *Treponema denticola*. Based on these results we identified a set of active site residues that are essential for specific ergothionase activity. These residues are strictly conserved many homologous proteins encoded predominantly in firmicutes and proteobacteria, and also in several pathogenic bacteria from other phyla.

Crystal structure of ergothionase. ETL from *T. denticola* (*Td*ETL, acession number: WP_010693216) was identified based on its sequence similarity to *Bu*ETL (34 % sequence identity).[10] The codon-optimized gene for *Td*ETL was expressed from a modified pET19(+) vector in *Escherichia coli* and purified following standard protocols (see supporting information). Crystals of *Td*ETL in native form and in complex with **8** were grown in tris-buffered solutions (pH 7.4) containing PEG4000, PEG200 and $CaCl_2$. One diffraction data set with a resolution of 2.1 Å was used to solve the structure of native *Td*ETL by molecular replacement (Table S1). The structure of the *Td*ETL:**8** complex was solved to a resolution of 2.6 Å using the native structure as a template. The electron densities of the two *Td*ETL structures reveal a continuous polypeptide chain from Asp2 to Ile498 (Figure 2 and S6). The overall structure of *Td*ETL is strikingly similar to that of histidine ammonia lyase (HAL, PDB: 1B8F, Figure S7) from *Pseudomonas putida*.[11] The backbones of the two proteins superimpose with an RMSD of 1.58 Å over 393 residues, despite sharing only 26 % sequence identity. Four largely α-helical monomers form a tetramer with *D*2 symmetry hosting four identical active sites that are lined by residues from three different monomers (Figure 2).

The crystal of the *Td*ETL:**8** complex contained residual electron density in the active site that allowed unambiguous placement of the ligand (Figure 2). Superposition of the native and the liganded structures shows no indication of conformational change upon ligand binding, suggesting that the enzyme provides a highly preorganized substrate-binding pocket (Figure S6 and S8). The two N-α-methyl groups of **8** pack against the aromatic plane of Phe327 and make close contacts with the backbone carbonyl of Glu143 (2.7 Å & 2.8 Å). Surprisingly, Glu143 adopts a conformation that points the sidechain away from the dimethyl amino moiety, indicating that the amino group of the substrate may not be protonated in the complex and therefore does not require stabilization by a complementary charge. The carboxylate of **8** approaches the side chains of Arg281 (3.7 Å) and Asn311 (3.5 Å), but the rather long distances suggest that electrostatic interactions may be more important than hydrogen-bonding. The aromatic plane of the imidazole ring is squeezed between the hydrophobic side chains of Val60 and Ile146. The two imidazole N-H groups of **8** interact with the hydrogen bond acceptors Glu412 (Nπ, 2.8 Å) and His84 (Nτ, 3.2 Å). His84 also hydrogen bonds with Ser83 which in turn hydrogen bonds with the backbone carbonyl of Asn79 (Figure 2). This hydrogen bonded triad stabilizes His84 as a hydrogen-bond acceptor with respect to ligand **8**. The sulfonic acid moiety hydrogen bonds with the side chains of Thr381 and Lys384. Finally, the phenol function of Tyr54 hovers right above the β-methylene group of **8**, well-positioned for abstraction of the pro-S proton from the substrate. Structurally equivalent tyrosine residues have been identified as the catalytic base in HAL and related ammonia lyases and mutases.[11-12] A model of *Td*ETL in complex with **1** shows that the native substrate

Table 1.[a]

entry	enzyme	substrate	k_{cat} [s^{-1}]	k_{cat}/K_M [$s^{-1}M^{-1}$]
AA	*Td*ETL$_{wt}$	**1**	64 ± 3	1.4 x 10^6
BB	*Td*ETL$_{Y54F}$	**1**	0.02 ± 0.001	6.5 x 10^2
EC	*Td*ETL$_{K384M}$	**1**	0.02 ± 0.01	5.0 x 10^2
DD	*Td*ETL$_{E412Q}$	**1**	0.05 ± 0.01	2.4 x 10^2
CE	*Td*ETL$_{K64M}$	**1**	0.11 ± 0.01	1.1 x 10^5
FF	*Td*ETL$_{wt}$	**3**	17 ± 1	1.1 x 10^5
GG	*Td*ETL$_{Y54F}$	**3**	0.003 ± 0.001	1.7 x 10^1
IH	*Td*ETL$_{K384M}$	**3**	0.005 ± 0.001	2.8 x 10^0
HI	*Td*ETL$_{E412Q}$	**3**	0.002 ± 0.001	4.6 x 10^2
JJ	*Td*ETL$_{wt}$	**2**	0.04 ± 0.002[b]	-
K	*Td*ETL$_{wt}$	**4**	0.001[b]	-
L	*Td*ETL$_{K384M}$	**2**	0.2 ± 0.01[b]	-
M	*Td*ETL$_{K384M}$	**4**	0.09 ± 0.001[b]	-
N	*Td*ETL$_{wt}$	**8**	0.0022[b]	-
O	*Td*ETL$_{wt}$	**9**	0.012[b]	-
P	*Td*ETL$_{wt}$	histidine	0.0001[b]	-

[a] Displayed values represent averages from three independent measurements. The corresponding Michaelis-Menten plots are shown in the supporting information. Initial rates determined at different $[S]_{t=0}$ were fitted with $v = k_{cat}[S]/(K_M + [S])$. [b] These parameters correspond to $k_{obs} = (dP/dt)_{obs}/[S]_{t=0}$, determined at a $[S]_{t=0}$ = 2 mM.

can make the same contacts with the active site (Figure S9, Figure 3). In particular, the enzyme appears to accommodate the difference between the imidazole sulfonic acid side chain of **8** and the 2-mercaptoimidazole of **1** with minimal conformational change.

Kinetic characterization. To examine how this active site catalyzes the elimination of trimethylamine from **1** we measured the activity of *Td*ETL using a UV-Vis based assay that monitors production of **5** in a HEPES-buffered solution at pH 7.5 and 23°C (Figure S11). Under these conditions *Td*ETL-catalyzed production of **5** is characterized by a k_{cat} of 64 s^{-1} and a catalytic efficiency (k_{cat}/K_M) of 1.4 x 10^6 $M^{-1}s^{-1}$ (Table 1, entry A). The pH-dependence of k_{cat} follows a bell-shaped curve with a maximum near 7.5 (pK_{a1} = 6.6 ± 0.1, pK_{a2} = 8.7 ± 0.1, Figure S12 and S13). This behavior is diagnostic for a mechanism that depends on general acid and base catalysis. Measuring *Td*ETL activity with deuterated **1** revealed a primary substrate kinetic isotope effect (KIE) of 1.8 ± 0.2 on k_{cat}, suggesting that base-catalyzed C-H bond cleavage is partially rate limiting. In contrast, k_{cat}/K_M is much less affected by substrate deuteration (KIE = 1.2 ± 0.1), suggesting that C-H bond cleavage is not rate limiting at low substrate concentrations (Figure S14). The most likely interpretation of this behavior is that substrate-unbinding is slow relative to the forward reaction (C-H cleavage), which makes substrate binding essentially irreversible.[13] Independent of this interpretation, these results highlight that for *Td*ETL the K_M is not a measure of substrate affinity ($K_S = k_{off}/k_{on}$) but instead is dominated by the ratio between k_{cat} and the rate of substrate binding ($K_M = k_{cat}/k_{on}$).

In a next step we probed the effect of three mutations that eliminate polar interactions between the enzyme and the ligand. Mutation of Tyr54 to Phe, Lys384 to Met, and Glu412

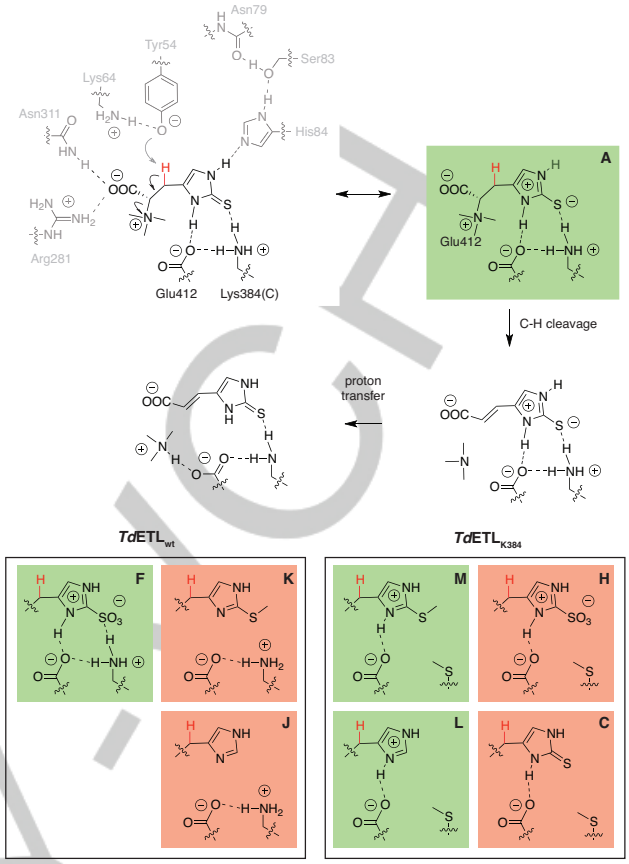

Figure 3. Top: Proposed substrate binding mode and mechanism for substrate activation by *Td*ETL$_{wt}$. **Bottom:** Charge complementary enzyme:ligand complexes that stabilize a positive charge on the imidazole ring (green) are more active that complexes with unbalanced charge or a neutral imidazole ring (red). Bold letters indicate the corresponding entry in table 1

to Gln each reduced k_{cat} and catalytic efficiency by over three orders of magnitude (entries B, C and D, Table 1). These strong effects demonstrate that the three residues are absolutely essential for catalysis. In contrast, mutation of Lys64 to Met decreased catalytic efficiency only by 10-fold (entry E). In the *Td*ETL:**8** complex and the native structure Lys64 adopts a conformation that points the side chain toward the protein exterior (Figure 2, Figure S6). However, the electron density of a second native crystal indicates an alternative conformation of Lys64 placing the ε-amino function of the side chain in proximity to the phenol function of Tyr54 (Figure S8). Hence, in this conformation Lys64 could suppress the pK_a of Tyr54 and therefore activate this residue as a catalytic base. Consistently, mutation of Lys64 to Met resulted in a *Td*ETL variant with a pH optimum that is 1.5 units higher than that of wild type (pK_{a1} = 8.2 ± 0.2, pK_{a2} = 9.5 ± 0.1, Figure S15 and S16). Comparison of the wild type and variant pH-dependence curves showed that this shift is predominantly due to an increase of pK_{a1} (Figure S17).

Substrate specificity profile of *Td*ETL. As a complementary approach to study enzyme:substrate interactions that are important for ETL-activity, we examined the range of accepted substrate analogs. Most interestingly, **3** is consumed by *Td*ETL with a catalytic efficiency only ten-fold lower than measured for **1** (entry F, Table 1). Mutation of residues Tyr54, Lys384 and Glu412 caused similar reduction

of the catalytic efficiency for **3** (entries G, H, I), corroborating the proposition that **1** and **3** make similar interactions with the active site (Figure S18). Apparently, the relatively bulky and anionic head group is well tolerated by the enzyme. In contrast, N-α-trimethylhistidine (**2**) and S-methyl ergothioneine (**4**) are both poor substrates (entries J and K) even though they seem structurally more similar to **1**. Also, desmethyl ergothioneine (**9**) and desmethyl ergothioneine sulfonic acid (**8**) are poor substrates (entries N and O) despite having identical side chains as **1** and **3**. Finally, histidine is turned over almost 10^6-fold slower that the native substrate **1** (entry P) underscoring the functional difference between ergothionases and histidine ammonia lyases.[10]

Mechanisms of substrate activation. The ability of *Td*ETL to accept **3** as an alternative substrate while rejecting **2**, **4**, **8** and **9** provides important clues as to how the enzyme binds and activates its native substrate **1**. The structure of *Td*ETL:**8** and the efficient turnover of **3** suggests that the active site is well-equipped to solvate the zwitterionic side chain with a positive charge on the imidazolium ring and an anionic head group (Figure 3F). The native substrate **1** can be drawn as a resonance structure with the same zwitterionic charge distribution that can also interact with Glu412 and Lys384 to form an overall neutral complex (Figure 3A). The positive charge on the imidazole ring inevitably renders the adjacent β-methylene group more acidic which likely activates the substrate for base-catalyzed proton abstraction. This activation mechanism seems crucial for catalysis. Compounds **2** and **4** cannot attain a zwitterionic state, forcing these ligands to bind with a neutral side chain. Hence the β-methylene group of these substrates remain unactivated (Figure 3K and 3J). Consistent with this model, we found that the variant *Td*ETL$_{K384M}$ which lacks one positive charge and may therefore bind the imidazole rings in protonated form, consumes **2** and **4** 5- and 90-fold more efficiently than the wild type (Figure 3L and 3M). The fact that the Lys384Met mutation decreased the catalytic efficiency for **1** and **3** by three orders of magnitude underscores the importance of charge complementarity between the active site and the substrate with a protonated imidazole ring (Figure 3C & 3H).

The observation that **8** and **9** are also poor substrates highlights a second contribution to substrate activation. The structure of the *Td*ETL:**8** complex shows that the dimethyl amino group is buried in a relatively non-polar and neutral pocket that provides no direct counterion to stabilize the cationic charge of a protonated amine. **8** and **9** can accommodate by binding with a neutral α-amino group. However, neutral dimethyl amine is a poor leaving group. Consequently, turnover of **8** and **9** is barely measurable Table 1). By contrast, binding of the substrates **1** and **3** forces the quaternary ammonium group into the same apolar pocket which likely increases the leaving group ability of this moiety. In summary, the structure and substrate specificity profile of *Td*ETL show that this enzyme activates its substrate by a) polarization of the side chain and b) destabilization of the leaving group. If either of the two activation modes is inaccessible, catalysis is three orders of magnitude less efficient.

ETL in commensal and pathogenic bacteria. The four residues we found essential for catalysis in *Td*ETL are strictly conserved in 260 homologous proteins (UniProt database) encoded by proteobacteria (163), firmicutes (73), synergistetes (16), and miscellaneous species from other phyla (Table S3). This group includes many gastrointestinal bacteria such as *Blautia spp*., *Clostridium spp*., *Paenibacillus spp*., *Peptoniphilus spp*., *Campylobacter spp*., and *Escherichia spp*., indicating that non-oxidative degradation of **1** is a common trait in the gut microbiome.[14] Although the quantitative aspects of ergothioneine breakdown in the gastrointestinal tract have yet to be explored, it seems possible that the composition of the gut microbiome may be a factor in determining the availability of this vitamin for the host. In addition, the ETL product trimethylamine and particularly its oxidative degradation product trimethylamine N-oxide (TMAO) have been linked to medical problems such as nonalcoholic fatty acid liver disease and cardiovascular disease.[15] Hence, overconsumption of ergothioneine as a food additive may have undesirable side effects.

The presence of ETL homologs in numerous pathogens, such as *Chlamydia trachomatis*, *Fusobacterium nucleatum*,[16] *T. denticola*,[17] or *B. pseudomallei*,[18] raise the additional possibility that ergothioneine degradation may contribute to the virulence and persistence of these bacteria in human tissue. For example, *T. denticola* participates in bacterial consortia that are associated with chronic inflammation of the periodontal tissues.[19] One factor that contributes to virulence of *T. denticola* is the conversion of glutathione to hydrogen sulfide which can affect host tissue as cytotoxin, or can dysregulate the host defense systems by activating both pro- and anti-inflammatory mechanisms.[20] ETL activity may allow *T. denticola* and other oral pathogens to recruit ergothioneine as an alternative sulfur source in the progression of periodontal disease.

Conclusions. In this report we described the crystal structure of ETL from the human pathogen *T. denticola* in complex with the slow substrate analog desmethyl ergothioneine sulfonic acid. This structure, combined with the catalytic activities of the wild type enzyme and active site variants identified a set of polar interactions between the enzyme and its substrate that are essential for catalysis. The same active site configuration occurs in homologous proteins encoded in 260 bacterial genomes. This work paves the way to investigate the potential impact of bacterial ergothioneine degradation on human health. The discovery that many common members of the gut microbiome catabolize **1** to the problematic metabolite trimethylamine may provide a cautionary corrective to the increasing advertisements of this natural product as a food additive. On a different note, the structure and mechanistic characterization of *Td*ETL opens the door for comparison to related enzymes such as HAL or aspartate ammonia-lyase that catalyze similar 1,2-elimination reactions but use different mechanisms for substrate activation.[11-12, 21]

Acknowledgements

The authors thank Dr. Jean-Claude Yadan (Tetrahedron) for the kind gift of compounds **1**, **3** and **8**. This project was supported by the Swiss National Science Foundation, the University of Basel, the NCCR for Molecular Systems

Engineering, the “Professur für Molekulare Bionik” and a starting grant from the European Research Council (ERC-2013- StG 336559). We thank the Swiss Light Source (SLS Villigen, Switzerland) for access to facilities and beamline staff for support.

Keywords: ergothioneine • microbiome • ammonia-lyase • *Treponema denticola* • enzymology • crystallography

[1] aB. Halliwell, I. K. Cheah, R. M. Y. Tang, *FEBS Lett.* **2018**, *592*, 3357 - 3366; bB. Halliwell, I. K. Cheah, C. L. Drum, *Biochem. Biophys. Commun.* **2016**, *470*, 245 - 250; cI. K. Cheah, R. Tang, P. Ye, T. S. Z. Yew, K. H. C. Lim, B. Halliwell, *Free Radic. Res.* **2016**, *50*, 14 - 25; dT. Y. Song, H. C. Lin, C. L. Chen, J. H. Wu, J. W. Liao, M. L. Hu, *Free. Radic. Res.* **2014**, *48*, 1049 - 1060; eY. Kato, Y. Kubo, D. Iwata, S. Kato, T. Sudo, T. Sugiura, T. Kagaya, T. Wakayama, A. Hirayama, M. Sugimoto, K. Sugihara, S. Kaneko, T. Soga, M. Asano, M. Tomita, T. Matsui, M. Wada, A. Tsuji, *Pharm. Res.* **2010**, *27*, 832 - 840; fI. K. Cheah, L. Feng, R. M. Tang, K. H. Lim, B. Halliwell, *Biochem. Biophys. Res. Commun.* **2016**, *478*, 162 - 167; gJ. Ey, E. Schomig, D. Taubert, *J. Agric. Food Chem.* **2007**, *55*, 6466-6474; hR. W. Li, C. Yang, A. S. Sit, Y. W. Kwan, S. M. Lee, M. P. Hoi, S. W. Chan, M. Hausman, P. M. Vanhoutte, G. P. Leung, *J. Pharmacol. Exp. Ther.* **2014**, *350*, 691 - 700; iL. Feng, I. K. Cheah, M. M. Ng, J. Li, S. M. Chan, S. L. Lim, R. Mahendran, E. H. Kua, B. Halliwell, *J Alzheimers Dis.* **2019**, *68*, 197 - 203.

[2] aD. Gründemann, S. Harlfinger, S. Golz, A. Geerts, A. Lazar, R. Berkels, N. Jung, A. Rubbert, E. Schoemig, *Proc. Natl. Acad. Sci. U. S. A.* **2005**, *102*, 5256-5261; bJ. Tschirka, M. Kreisor, J. Betz, D. Gründemann, *Drug Metab Dispos.* **2018**, *46*, 779 - 785.

[3] D. Gründemann, *Prev. Med.* **2012**.

[4] Y. Tang, Y. Masuo, Y. Sakai, T. Wakayama, T. Sugiura, R. Harada, A. Futatsugi, T. Komura, N. Nakamichi, H. Sekiguchi, K. Sutoh, K. Usumi, S. Iseki, S. Kaneko, Y. Kato, *J Pharm Sci.* **2016**, *105*, 1779 - 1789.

[5] B. N. Ames, *Proc Natl Acad Sci U S A.* **2018**, *115*, 10836 - 10844.

[6] aA. Askari, D. B. Melville, *J. Biol. Chem.* **1962**, *237*, 1615-&; bF. P. Seebeck, *J. Am. Chem. Soc.* **2010**, *132*, 6632-6633; cR. Burn, L. E. Misson, M. Meury, F. P. Seebeck, *Angew Chem Int Ed Engl.* **2017**, *56*, 12508 - 12511.

[7] aA. Stampfli, K. V. Goncharenko, M. Meury, B. Dubey, T. Schirmer, F. P. Seebeck, *J Am Chem Soc* **2019**, *141*, 5275 - 5285; bA. Vit, L. E. Misson, W. Blankenfeldt, F. P. Seebeck, *ChemBioChem* **2015**, *16*, 119 - 125; cF. Leisinger, R. Burn, M. Meury, P. Lukat, F. P. Seebeck, *J. Am. Chem. Soc.* **2019**, *141*, 6906 - 6914; dK. V. Goncharenko, A. Vit, W. Blankenfeldt, F. P. Seebeck, *Angew. Chem. Int. Ed. Engl.* **2015**, *54*, 2821 - 2824; eS. Irani, N. Naowarojna, Y. Tang, K. R. Kathuria, S. Wang, A. Dhembi, N. Lee, W. Yan, H. Lyu, C. E. Costello, P. Liu, Y. J. Zhang, *Cell Chem Biol.* **2018**, *25*, 519 - 529; fC. Liao, F. P. Seebeck, *ChemBioChem* **2017**, *18*, 2115 - 2118; gA. Vit, G. T. Mashabela, W. Blankenfeldt, F. P. Seebeck, *ChemBioChem* **2015**, *16*, 1490 - 1496.

[8] L. Servillo, D. Castaldo, R. Casale, N. D'Onofrio, A. Giovane, D. Cautela, M. L. Balestrieri, *Free Radic. Biol. Med.* **2015**, *79*, 228 - 236.

[9] aJ. B. Wolff, *J. Biol. Chem.* **1962**, *237*, 874 - 881; bD. Yanasugondha, M. D. Appleman, *J. Bacteriol.* **1957**, *74*, 381 - 385; cB. Kelly, M. D. Appleman, *J Bacteriol* **1961**, *81*, 715 - 720.

[10] H. Muramatsu, H. Matsuo, N. Okada, M. Ueda, H. Yamamoto, S. Kato, S. Nagata, *Appl Microbiol Biotechnol.* **2013**, *97*, 5389 - 5400.

[11] T. F. Schwede, J. Rétey, G. E. Schulz, *Biochemistry* **1999**, *38*, 5355 - 5361.

[12] aS. D. Bruner, H. Cooke, *Biopolymers* **2010**, *93*, 802 - 810; bN. J. Weise, S. T. Ahmed, F. Parmeggiani, J. L. Galman, M. S. Dunstan, S. J. Charnock, D. Leys, N. J. Turner, *Sci Rep.* **2017**, *7*, 13691; cG. G. Wybenga, W. Szymanski, B. Wu, B. L. Feringa, D. B. Janssen, B. W. Dijkstra, *Biochemistry* **2014**, *53*, 3187 - 3198; dA. C. Schroeder, S. Kumaran, L. M. Hicks, R. E. Cahoon, C. Halls, O. Yu, J. M. Jez, *Phytochemistry* **2008**, *69*, 1496 - 1506.

[13] D. L. Purich, *Enzyme Kinetics*, Academic Press, London, **2010**.

[14] M. Rajilić-Stojanović, W. M. de Vos, *FEMS Microbiol Rev.* **2014**, *38*, 996 - 1047.

[15] aS. Rath, B. Heidrich, D. H. Pieper, M. Vital, *Microbiome.* **2017**, *5*; bW. H. W. Tang, D. Y. Li, S. L. Hazen, *Nat Rev Cardiol.* **2019**, *16*, 137 - 154; cS. H. Zeisel, M. Warrier, *Annu Rev Nutr.* **2017**, *37*, 157 - 181.

[16] S. Bullman, C. S. Pedamallu, E. Sicinska, T. E. Clancy, X. Zhang, D. Cai, D. Neuberg, K. Huang, F. Guevara, T. Nelson, O. Chipashvili, T. Hagan, M. Walker, A. Ramachandran, B. Diosdado, G. Serna, N. Mulet, S. Landolfi, Y. Ramon, S. Cajal, R. Fasani, A. J. Aguirre, K. Ng, E. Élez, S. Ogino, J. Tabernero, C. S. Fuchs, W. C. Hahn, P. Nuciforo, M. Meyerson, *Science* **2017**, *358*, 1443 - 1448.

[17] H. G., *Nat Rev Immunol.* **2015**, *15*, 30 - 44.

[18] W. J. Wiersinga, H. S. Virk, A. G. Torres, B. J. Currie, S. J. Peacock, D. A. B. Dance, D. Limmathurotsakul, *Nat Rev Dis Primers.* **2018**, *4*.

[19] S. G. Dashper, C. A. Seers, K. H. Tan, E. C. Reynolds, *J. Dent. Res.* **2011**, *90*, 691 - 703.

[20] aH. Kimura, *Antioxid Redox Signal.* **2010**, *12*, 1111 - 1123; bL. Chu, Z. Dong, X. Xu, D. L. Cochran, J. L. Ebersole, *Infect Immun.* **2002**, *70*, 1113 - 1120.

[21] V. Puthan Veetil, G. Fibriansah, H. Raj, A. M. Thunnissen, G. J. Poelarends, *Biochemistry* **2012**, *51*, 4237 - 4243.

Entry for the Table of Contents (Please choose one layout)

Layout 1:

COMMUNICATION

Text for Table of Contents

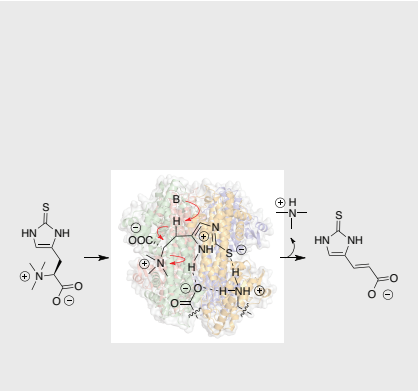

*Alice Maurer, Florian Leisinger, David Lim and Florian P. Seebeck**

Page No. – Page No.

Structure and mechanism of ergothionase from *Treponema denticola*